International Journal of Nanomedicine

Dovepress
open access to scientific and medical research

Open Access Full Text Article

ORIGINAL RESEARCH

Theranostic pH-sensitive nanoparticles for highly efficient targeted delivery of doxorubicin for breast tumor treatment

This article was published in the following Dove Press journal:
International Journal of Nanomedicine

Changqie Pan[1–3,*]
Yuqing Liu[2,3,*]
Minyu Zhou[1]
Wensheng Wang[4]
Min Shi[1]
Malcolm Xing[2,3,5]
Wangjun Liao[1]

[1]Department of Oncology, Nanfang Hospital, Southern Medical University, Guangzhou, China; [2]Department of Mechanical Engineering, [3]Department of Biochemistry and Medical Genetics, University of Manitoba, Winnipeg, MB, Canada; [4]The Imaging Center, 999 Brain Hospital, Guangzhou, China; [5]Children's Hospital Research Institute of Manitoba, Winnipeg, MB, Canada

*These authors contributed equally to this work

Abstract: A multifunctional theranostic nanoplatform integrated with environmental responses has been developed rapidly over the past few years as a novel treatment strategy for several solid tumors. We synthesized pH-sensitive poly(β-thiopropionate) nanoparticles with a supermagnetic core and folic acid (FA) conjugation (FA-doxorubicin-iron oxide nanoparticles [FA-DOX@IONPs]) to deliver an antineoplastic drug, DOX, for the treatment of folate receptor (FR)-overexpressed breast cancer. In addition to an imaging function, the nanoparticles can release their payloads in response to an environment of pH 5, such as the acidic environment found in tumors. After chemical (^{1}H nuclear magnetic resonance) and physical (morphology and supermagnetic) characterization, FA-DOX@IONPs were shown to demonstrate pH-dependent drug release profiles. Western blotting analysis revealed the expression of FRs in three breast cancer cell lines, MCF-7, BT549, and MD-MBA-231. The cell counting kit-8 assay and transmission electron microscopy showed that FA-DOX@IONPs had the strongest cytotoxicity against breast cancer cells, compared with free DOX and non-FR targeted nanoparticles (DOX@IONPs), and caused cellular apoptosis. The FA-DOX@IONP-mediated cellular uptake and intracellular internalization were clarified by fluorescence microscopy. FA-DOX@IONPs plus magnetic field treatment suppressed in vivo tumor growth in mice to a greater extent than either treatment alone; furthermore, the nanoparticles exerted no toxicity against healthy organs. Magnetic resonance imaging was successfully applied to monitor the nanoparticle accumulation. Our results suggest that theranostic pH-sensitive nanoparticles with dual targeting could enhance the available therapies for cancer.

Keywords: theranostics, magnetic nanoparticle, pH sensitivity, folate receptor targeting, breast cancer

Introduction

Breast cancer is the most commonly diagnosed carcinoma in women worldwide and a common cause of death in women.[1,2] The poor outcomes of patients with breast cancer, as reflected by inferior disease-free survival and overall survival rates,[3] are largely attributable to the highly adverse proliferation, invasion, and metastasis of breast cancer cells. There are numerous therapeutic methods for breast cancer in clinical practice: curative surgery, chemotherapy, radiation, hormonal therapy, and biologically targeted therapy. Of these, chemotherapy is widely used and has been established as a vital treatment for women with breast cancer.

The efficacy of doxorubicin (DOX) for the treatment of breast cancer has been demonstrated over several decades, although there is no single standard chemotherapy plan for clinical cancer treatments.[4] DOX can induce cardiotoxicity, gastrointestinal

Correspondence: Wangjun Liao
Department of Oncology, Nanfang Hospital, Southern Medical University, Guangzhou 510515, China
Fax +86 20 6278 7731
Email nfyyliaowj@163.com

Malcolm Xing
Department of Mechanical Engineering, University of Manitoba, Winnipeg, MB R3T 2N2, Canada
Fax +1 204 275 7507
Email malcolm.xing@umanitoba.ca

submit your manuscript | www.dovepress.com
Dovepress
http://dx.doi.org/10.2147/IJN.S147464

toxicity, and bone marrow suppression.[5–12] Nanoparticles, which are effective drug delivery platforms owing to their enhancement of antitumor efficacy, have been welcomed for their efficient cellular uptake, controllable release, and higher drug accumulation.[13–15] Moreover, given the appropriate physical design and synthetic versatility, an increasing number of surface coatings can be modified to yield environmentally sensitive nanoparticles with superior performance. Many previous studies have reported that drug delivery vehicles with pH-sensitive chemical bonds accelerate drug delivery and cause release at a lower pH.[16,17]

Iron oxide nanoparticles (IONPs), a promising magnetic resonance imaging (MRI) agent, are extensively used in the field of cancer theranostics; they facilitate the description of targeted therapeutic drugs and the diagnosis of the lesion areas.[18,19] Researchers have verified that external magnetic induction allows DOX-containing nanoparticles to preferentially concentrate at the tumor site, and thereby increase the drug levels for an enhanced therapeutic effect.[20–22] Notably, folate-conjugated particles have promisingly displayed a high and initiative targeting efficacy to folate receptor (FR)-overexpressing xenografted tumors,[23–25] which has resulted in improved chemotherapeutic effects.[26] Despite these advances, the comparison and synergetic effects of the magnetic field, active targeting, and environmental response-based delivery to breast tumor have not yet been fully studied.

We report the development of a targeted folic acid (FA)-DOX@IONP-based drug delivery system for cancer theranostics that encompasses three properties: FR targeting, the pH sensitivity of poly(β-thiopropionate) with two acid-sensitive structures including thiopropionate and aminoester, and magnetic targeting/imaging. Aminoester groups are weakly basic owing to their tertiary amine groups, which are protonated to become a positively charged salt and water soluble in a low-pH environment, in contrast to their water insolubility in neutral solutions.[27] The β-thiopropionate unit is acid-labile and cleaved at pH 5.5.[28] In this study, both components were used simultaneously to promote the pH responsiveness of self-assembled amphiphilic polymer nanoparticles to achieve controlled drug release in the acidic environment of tumors. We confirmed the potent antitumor activity of FA-DOX@IONPs both in vivo and in vitro and studied their structural and biomedical characteristics. Using this method, we developed an effective approach for the production of FA-DOX@IONPs, which could potentially maximize the therapeutic effects and minimize side effects to healthy organs, for targeted antitumor drug delivery, with appropriate pH sensitivity and high DOX loading.

Materials and methods

All chemicals for the synthesis of polymeric nanoparticles were obtained from Sigma-Aldrich Co (St Louis, MO, USA). DOX was obtained from Santa Cruz Biotechnology Inc (Dallas, TX, USA). The cell counting kit-8 (CCK8) kit was purchased from Beyotime Institute of Biotechnology (Shanghai, China). 3,3′-dioctadecyloxacarbocyanine perchlorate (DIO) and 4′,6-diamidino-2-phenylindole (DAPI) dye liquor, hematoxylin and eosin (H&E), and Prussian blue were obtained from Sigma-Aldrich Co. Fetal bovine serum (FBS), trypsin/EDTA, and phosphate-buffered saline (PBS) were obtained from Hyclone Laboratories, Logan, UT, USA. FA-deficient Dulbecco's Modified Eagle's Medium (DMEM) was obtained from Thermo Fisher Scientific, Waltham, MA, USA. The primary antibodies of FR and α-actin were obtained from Abcam (Cambridge, UK). The secondary antibody was obtained from Odyssey (Lincoln, NE, USA). All chemical reagents used for the Western blotting analysis were obtained from Beyotime Institute of Biotechnology.

Methoxypolyethylene glycol (PEG) amine and hydrochloride (HCl) salt (molecular weight [MW] =5,000 Da) were purchased from JenKem Technology (Beijing, China). Double-distilled (DD) water (ultrapure water, 18.2 MΩ) was purified by using a Direct-Q®3 instrument (EMD Millipore, Billerica, MA, USA).

Synthesis of cysteamine (CY) capped tetra (ethylene glycol) (CY-TEG)

In a 20 mL glass vial, 2-aminoethanethiol HCl (CY HCl, 568 mg, 5 mmol), tetra (ethylene glycol) diacrylate (756 mg, 2.5 mmol), and trimethylamine (25.3 mg, 0.25 mmol) were dissolved in 10 mL methanol and stirred at 25°C overnight. The solvent was then removed by rotary evaporation; a small aliquot dried completely under vacuum was used to obtain the ^{1}H nuclear magnetic resonance (^{1}H NMR) spectrum directly. The product was dissolved in dichloromethane (DCM), mixed with saturated $NaHCO_3$ solution to remove HCl, and washed with a saturated brine solution. The organic layer was dried first over anhydrous Na_2SO_4 and then completely dried in vacuum to yield a colorless oil (1.1 g, 83%). ^{1}H NMR (ppm) in deuterium oxide (D_2O): δ2.70–2.82 ppm (t, −OOC−***CH$_2$***−CH_2−S−), δ2.83–2.95 ppm (m, −CH_2−***CH$_2$***−S−***CH$_2$***−), δ3.20–3.30 ppm (t, −S−CH_2−***CH$_2$***−NH_2), δ3.68–3.78 ppm (s, −O−***CH$_2$***−***CH$_2$***−O−), δ3.78–3.88 ppm (m, −COO−CH_2−***CH$_2$***−), δ4.28–4.38 ppm (m, −COO−***CH$_2$***−CH_2−). In the text, the bolded and italicized protons (H, hydrogen) are the specific protons assigned to the discussed peak ranges. To locate accurately the specific protons in some

similar chemical structures, we have to provide those protons and their neighbor chemical groups. So it is necessary to bold and italicize the targeted protons to make them different from their neighbor groups; ie, the peak regions are relative to the hydrogens in bold and italic forms only.

Synthesis of CY-TEG-diacrylate (CY-TEG-DA)

First, 912 mg of CY-TEG (2 mmol) and 0.62 mL triethylamine (TEA, 4.4 mmol) were dissolved in 10 mL anhydrous DCM and degassed by N_2 sparging for 15 minutes in an ice bath. Next, 0.36 mL acryloyl chloride (4.4 mmol) was added dropwise to the solution, which was stirred at 0°C for 3 hours and then gradually increased to ambient temperature. After 24 hours, the reaction was stopped, and the solution was washed sequentially with saturated $NaHCO_3$ and NaCl. The DCM solution was dried over anhydrous Na_2SO_4 powder until a clear solution was obtained. After evaporation of the solvent, a light-yellow viscous oil was collected with a yield of 0.8 g (70%). The product was used for the next step in the reaction without further purification. ^{1}H NMR (ppm) in chloroform-d ($CDCl_3$): δ2.50–3.00 ppm (m, –OOC–***CH_2***–CH_2–S–, CH_2–***CH_2***–S–***CH_2***–), δ3.40–3.80 ppm (m, –S–***CH_2***–CH_2–NH_2–CO–, –O–***CH_2***–***CH_2***–O–, –COO–CH_2–***CH_2***–O–), δ4.15–4.3 ppm (m, –COO–***CH_2***–CH_2–O–), δ5.60–6.50 ppm (m, ***CH_2***=***CH***–CONH–).

Synthesis of poly(β-thiopropionate) amphiphilic copolymer

For synthesis, 565 mg CY-TEG-DA (1 mmol), 126 mg dodecylamine (0.68 mmol), 29 mg 5-aminopentanol (0.28 mmol), and 250 mg methoxy PEG amine (molecular weight 5,000 Da, 0.05 mmol) were dissolved in 2 mL methanol in a 20 mL clear glass vial. The resulting clear solution was stirred at 50°C for 3 days, and the reaction was terminated by pouring the solution into 200 mL diethyl ether to obtain a light-yellow precipitate. The product was redissolved in 2 mL DCM and reprecipitated in 200 mL diethyl ether to remove any unreacted small molecules. The dried product was dissolved in DD water and dialyzed against DD water in a dialysis tube with a MW cutoff of ~6–8 kDa, for 2 days in a 10 L bucket with the water being changed frequently. The product was lyophilized to produce a white solid (yield 620 mg, 63%). ^{1}H NMR (ppm) in chloroform-d ($CDCl_3$): δ0.75–0.90 ppm (t, –CH_3), δ1.15–1.65 ppm (m, –N–CH_2–(***CH_2***)$_{10}$–CH_3), δ2.50–3.00 ppm (m, –N–CH_2–CH_2–CONH–, –OOC–CH_2–CH_2–S–, CH_2–CH_2–S–CH_2–, –N–***CH_2***–), δ3.38 ppm (s, –O–CH_3), δ3.40–3.50 ppm (m, N–(C_4H_8)–CH2–OH), δ3.55–3.80 ppm (m, –N–CH_2–CH_2–CONH–, –S–CH_2–***CH_2***–NH_2–CO–, –O–***CH_2***–***CH_2***–O–, –COO–CH_2–***CH_2***–O–), δ4.15–4.3 ppm (m, –COO–***CH_2***–CH_2–O–), δ0.75–0.90 ppm (t, –***CH_3***), δ1.15–1.65 ppm (m, –N–CH_2–(***CH_2***)$_{10}$–CH_3, –N–CH_2–(***CH2***)$_3$–CH_2OH), δ2.50–3.00 ppm (m, –N–CH_2–***CH_2***–CONH–, –OOC–***CH_2***–CH_2–S–, CH_2–***CH_2***–S–***CH_2***–), δ3.38 ppm (s, –O–***CH_3***), δ3.40–3.50 ppm (t, –***CH_2***–OH), δ3.55–3.80 ppm (m, –N–***CH_2***–CH_2–CONH–, –S–CH_2–***CH_2***–NH_2–CO–, –O–***CH_2***–***CH_2***–O–, –COO–CH_2–***CH_2***–O–), δ4.15–4.3 ppm (m, –COO–***CH_2***–CH_2–O–).

Synthesis of FA-conjugated poly(β-thiopropionate) amphiphilic copolymer

Two hundred milligrams of CY-TEG-PEG-poly(β-aminoester), 40 mg FA (0.09 mmol), 25 mg 1-ethyl-3-(3-dimethylaminopropyl) carbodiimide HCl (0.12 mmol), and 15 mg 4-dimethylaminopyridine (DMAP, 0.12 mmol) were dissolved in 8 mL N-methyl-2-pyrrolidone (NMP) and stirred at 25°C for 2 days. The reaction was terminated by the addition of 10 mL DD water, and the resulting yellow mixture was transferred into a dialysis tube with a MW cutoff of 6–8 kDa and dialyzed against DD water for 3 days. After lyophilization, a yellow solid was recovered (yield ~170 mg, 71%). ^{1}H NMR (ppm) in dimethyl sulfoxide (DMSO)-d_6: δ4.15 (s, –NH–***CH_2***–C(=N)–, COO–***CH_2***–), δ4.50 (–NH–***CH***–COOH), δ6.63, δ6.90, δ7.43, δ7.68 (m, NH–***C_6H_4***–CONH–), δ8.65 (s, N=***CH***–C(=N)–) were attributed to folate and the other peaks refer to poly(β-thiopropionate) amphiphilic copolymers.

Synthesis of superparamagnetic nanoparticles

Magnetic IONPs were synthesized in accordance with a previous protocol with some modifications.[29] Briefly, $Fe(NO_3)_3{\cdot}9H_2O$ (1.15 g, 2.9 mmol) and $FeSO_4{\cdot}7H_2O$ (0.4 g, 1.44 mmol) were added to a round-bottomed flask sealed with Suba Seal rubber septa cap (Sigma-Aldrich) and degassed with nitrogen for 15 minutes. DD water (10 mL) was injected to dissolve the compounds, and the obtained solution was degassed by N_2 sparging for another 15 minutes. The solution was heated to 45°C with vigorous stirring of 750 rpm, and nitrogen degassed ammonium oxide aqueous solution (1.25 mL, 25%) was rapidly injected into the flask with a syringe. After 30 minutes, 0.5 mL degassed oleic acid was transferred to the solution, under N_2 protection, and the reaction temperature was raised to 80°C for a further 1 hour. The magnetic nanoparticles were collected by a magnetic stirrer bar, washed several times with DD water and ethanol,

respectively, and finally dried in a vacuum oven at 25°C to yield a black wax-like solid.

Preparation of DOX and IONPs-loaded micelles

Briefly, in a 20 mL glass vial, 2 mg DOX, 0.6 μL TEA (1.5 eq), 2 mg magnetic nanoparticles, and 20 mg folate-conjugated poly(β-thiopropionate) were completely dissolved in 3 mL chloroform by stirring for ~1 hour at ambient temperature. DD water (5 mL) was added to the chloroform solution, and the mixture solution was sparged with nitrogen gas overnight to achieve complete removal of chloroform. The obtained brown solution was dialyzed through a membrane with an MW cutoff of ~6–8 kDa against DD water at 4°C for 24 hours. After lyophilization, the red solid powders were obtained with a yield of 20.2 mg. To examine the loading efficiency, 1 mg of the product was dissolved in 1 mL dimethylformamide to obtain a clear solution and an ultraviolet–visible (UV-vis) spectrometer was used to measure its absorption intensity at 480 nm. Based on a standard calibration curve of DOX, the drug entrapment efficiency was calculated to be 42% and the actual drug loading capacity was calculated as 3.5% for FA-DOX@IONPs. The control group DOX@IONPs were prepared by using the same protocol with a poly(β-thiopropionate) amphiphilic polymer; the drug entrapment efficiency was 39% and the corresponding drug loading capacity was 3.25%.

NMR characterization

^{1}H NMR experiments were performed on a Bruker Avance 300 MHz NMR Spectrometer (Bruker, Billerica, MA, USA). The samples were prepared in D_2O, chloroform-d, or DMSO-d_6 solution at 20 mg/mL and the experiment relaxation delay (d1) was 2 seconds.

Tumor cell lines and cell culture

The human breast cancer cell lines, MCF-7, MDA-MB-231, and BT549, were obtained from American Type Culture Collection (ATCC, Manassas, VA, USA) and cultured in accordance with ATCC protocols. The cells were maintained in FA-deficient DMEM supplemented with antibiotics (100 U/mL penicillin and 100 U/mL streptomycin) and 10% FBS (Hyclone, Thermo Fisher Scientific). The three cell lines were incubated in a humidified atmosphere containing 5% CO_2 at 37°C.

Western blotting analysis

The total proteins were extracted by using lysis buffer (Beyotime Institute of Biotechnology), and the protein concentration was measured by using the BCA Protein Assay Reagent Kit (Beyotime Institute of Biotechnology). The protein samples (50 mg) were electrophoresed on a 10% sodium dodecyl sulfate polyacrylamide gel electrophoresis separation gel, based on the MW of the target protein, and subsequently transferred onto polyvinylidene fluoride membranes (Immobilon P; EMD Millipore), in accordance with the manufacturer's protocol (Bio-Rad Laboratories Inc, Hercules, CA, USA). The membranes were incubated in 5% skim milk powder in Tris-buffered saline with Tween (TBST; 5% Tween-20) for 1 hour, with the primary antibodies at 4°C overnight, and with the fluorescent secondary antibodies at 25°C for 1 hour. Between each incubation, the membranes were washed three times with TBST. The images of the bands were obtained by using a near-infrared imaging system (Odyssey). Antibodies against FR were obtained from Abcam, and α-actin was used as a loading control.

CCK8 assay

The viability of drug-treated cells was quantified by using the CCK8 assay. MCF-7 cells (5×10^3 cells/well) were seeded into 96-well tissue culture plates in 200 μL complete FA-deficient medium and incubated for 24 hours at 37°C in 5% CO_2. After incubation, when a confluence of 60%–70% was reached, the cells were exposed to different concentrations of DOX (Santa Cruz Biotechnology Inc), DOX@IONPs, and FA-DOX@IONPs solutions at equivalent dosages of DOX (0, 1, 2.5, 5, 10, and 15 μg/mL) at pH 7.4. At the end of the exposure (24 hours), 20 μL CCK8 solution (Beyotime Institute of Biotechnology) was added to each well, and the cells were incubated at 37°C for a further 30 minutes and then analyzed by using a UV spectrophotometer (SpectraMax M5; Molecular Devices Corp., Sunnyvale, CA, USA) at 570 nm. Untreated wells were also treated with the same conditions and served as controls.

Establishment of breast tumor model and treatment

Female BALB/c nude mice (17±3 g, 4–5 weeks old) were purchased from the Laboratory Animal Center of Southern Medical University (SCXK 2011-0015; Guangzhou, Guangdong, China) and acclimatized for 10 days. MCF-7 human breast cancer cells (1×10^7) suspended in 150 mL PBS were inoculated subcutaneously into the right upper flanks of the 6-week-old BALB/c nude mice. When tumor sizes reached ~80 mm^3, the tumor-bearing mice were randomly divided into six groups (n=3 per group) for different therapeutic treatments. The mice in group 1 were injected with PBS as a negative control. The mice in groups 2–6 were administered

DOX, DOX@IONPs, FA-DOX@IONPs, DOX@IONPs, and FA-DOX@IONPs, respectively, with equivalent doses of DOX (7 mg/kg) diluted with 150 μL PBS. In addition, a magnet was immediately placed on the tumor surface for 1.5 hours after injection in groups 5 and 6. All injections were performed via the tail vein. All groups received the same treatments on day 0 and day 8. The tumor size (the longest =*a* and widest =*b* diameter) was measured using a caliper every other day until day 24, and the tumor volume (*v*) was calculated from the equation $v = a \times b^2/2$. The body weight of the mice was also monitored every other day until day 24.

The mice were maintained in cages and supplied with FA-deficient food and water ad libitum under a 12-hour light/dark cycle. All animal experimental procedures were performed in compliance with specific pathogen-free standards and the guidelines of the Laboratory Animal Center of Southern Medical University. All animal experiments were approved by the Animal Care and Use Committee of Nanfang Hospital, Southern Medical University.

Fluorescence microscopy assay

MCF-7 cells were seeded into 18-well tissue culture plates at a density of 1×10^5 cells/well in 500 μL of completely FA-deficient medium and then exposed to DOX, DOX@IONPs, and FA-DOX@IONPs at the same DOX concentration (7.5 μg/mL) for 2, 12, and 24 hours at different pH conditions (5.0 and 7.4). After three washes with PBS, the cells were stained with DIO and then DAPI in the dark for imaging of the cell membrane and nucleus, respectively. The images of the stained cells were captured by using an inverted fluorescence microscope (1X71; Olympus Corporation, Tokyo, Japan).

Immunohistochemistry

Immunohistochemical staining was conducted by using a Dako Envision System (Agilent Technologies, Santa Clara, CA, USA). Continuous 4-μm-thick sections of 4% paraformaldehyde-fixed, paraffin-embedded tumor tissues were cut and placed on slides. Each slice was treated with xylene twice for 15 minutes and then rehydrated by a graded series of ethanol/water (100%, 95%, 90%, 80%, and 70%). All slides were kept in 10 mM sodium citrate buffer, and then heat-induced antigen was retrieved by immersion in a boiling water bath for 3 minutes at 95°C. The slides were incubated with H_2O_2 to eliminate nonspecific staining. The sections were treated with a primary antibody, rat anti-mouse CD31 (PECAM-1) (1:100; Bioworld Technology Inc, St Louis Park, MN, USA), overnight at 4°C. The next day, the sections were washed three times with PBS for 5 minutes at 25°C and then incubated with a secondary antibody for 1 hour at 25°C. Tumor angiogenesis was detected by orange–brown staining (positive reactions). The stained slices were imaged by using a light microscope (Olympus 1X71). The value of the average microvessel density (AMVD) was calculated by manual counting under microscopy (each microscopic field was ~0.8 mm^2). Fifteen microscopic fields were selected at random for counting from each tumor sample.

H&E and Prussian blue staining assays

After the female BALB/c nude mice were sacrificed, the tissues from the tumor, heart, liver, and kidneys were isolated. All samples were fixed with 4% paraformaldehyde, embedded in paraffin, dehydrated, sliced into 4.0-μm sections, and then routinely subjected to Prussian blue and H&E staining studies in accordance with the recommended protocols. All the stained sample sections were examined by using a light microscope (Olympus 1X71).

MRI assay

The MRI experiments were conducted in nude mice with a body weight of ~18 g. Pentobarbital sodium (1%) diluted with PBS was used at a dose of 60 mg/kg body weight to anesthetize the mice before scanning. The mice were scanned before and after the administration of 150 μL of nanoparticles (70 mg [Fe]/kg body weight) for 12 and 24 hours via the tail vein. Coronal cross-sectional images were obtained from the MRI scanner (GE Healthcare Bio-Sciences Corporation, Piscataway, NJ, USA; 3.0 T superconducting unit, T2 sequence, slice thickness 1.0 mm).

In vitro drug release measurements

DOX-incorporated nanoparticles were added to dialysis bags in 30 mL PBS at pH 5.0 or 7.4 with a bed temperature incubator (37°C, 100 rpm). After incubation for 1, 2, 6, 12, 24, and 48 hours, 6 mL of the incubated solution was removed, and 6 mL fresh PBS was added to the dialysis tube to restore the volume of the dialysate to 30 mL. The removed solutions were subjected to UV-vis spectrometry at 480 nm, which is the wavelength of the maximum absorption of DOX in solution.

Dynamic light scattering (DLS)

The diameter and size distribution of the nanoparticles were measured by DLS (Malvern Instruments, Malvern, UK).

Transmission electron microscopy (TEM)

A scanning transmission electron microscope (Hitachi Ltd, Tokyo, Japan; H-7000FA, 75 kV) was used to observe the

morphology of nanoparticles and the apoptosis of MCF-7 cells treated with PBS or FA-DOX@IONPs (5 μg/mL) in folate-free media for 24 hours.

Vibrating sample magnetometer (VSM)

The magnetic properties of DOX@IONPs and FA-DOX@IONPs were examined by using a VSM.

Statistical analyses

The data are reported as mean ± standard deviation and were analyzed by two-way analysis of variance computed by SPSS 20.0 software (IBM Corporation, Armonk, NY, USA). Values of $p<0.05$ were considered statistically significant. All experiments were independently conducted three times.

Results and discussion

Synthesis and characterization of nanoparticles

The overall synthetic route for the preparation of poly(β-thiopropionate)-based amphiphilic polymers is presented in Figure 1. The β-thiopropionate functional moieties were prepared by the Michael addition reaction between the thiol groups of CY HCl and the acrylates of tetraethylene glycol diacrylate. The amine groups of CY were protected by HCl from reaction with acrylate. In this reaction, equal amounts of thiols and acrylates were added and a small amount of TEA was added as a catalyst to aid 100% conversion. After reaction, the solvent was removed, and the product was dried and dissolved in D_2O for direct NMR examination. The NMR spectrum, shown in Figure S1A, contained a blank region in the range 5.5–6.5 ppm, which was indicative of the complete consumption of acrylate groups and the completion of the thiol-ene addition. The resulting β-thiopropionate-containing diamine (CY-TEG) was reacted with acryloyl chloride to introduce acrylate groups to two sides of the compound, after mixing with $NaHCO_3$ to remove HCl and drying. In the NMR spectrum of the obtained β-thiopropionate-containing diacrylate (CY-TEG-DA) (Figure S1B), the peaks between 5.5 and 6.5 ppm were assigned to the protons on the carbon–carbon double bonds, which was indicative of the successful coupling of acrylates to CY-TEG. Moreover, in comparison with the spectrum of CY-TEG, the peak of $-S-CH_2-CH_2-NH_2$ completely shifted from 3.25 to 3.6 ppm after reaction because of the stronger electron-withdrawing ability of the formed imide functional groups, which showed that all the amines of CY-TEG reacted in this step. There was also some residual TEA·HCl impurities left for achieving a higher yield of products, which have little influence on the next step of the Michael addition reaction and could be easily removed by sequential dialysis.

Amphiphilic poly(β-thiopropionate) was synthesized by the Michael addition of β-thiopropionate containing diacrylate and various amines containing different pendants, including dodecyl groups, pentanol groups, and methoxy PEG groups. The introduced dodecyl groups form the hydrophobic side chains of the amphiphilic copolymers, the pentanol groups provide hydroxyl functional groups for conjugation with FA in subsequent steps, and the PEG side chains confer hydrophilicity to the polymer. The proton NMR spectrum of the product clearly indicated the existence of PEG side chains (3.65 ppm), β-thiopropionate units (2.5–3.0 ppm), and dodecyl and pentanol side chains (1.15–1.65 ppm), as shown in Figure S1C. To calculate the introduction rate of the dodecylamine, methoxy PEG amine, and 5-aminopentanol functionalities in the copolymers, we compared the peak intensities of the end groups of the side chains at 0.89, 3.38, and 3.45 ppm, respectively. The sharp peak at 0.89 ppm was assigned to three protons in the methyl group of dodecylamine. The tiny sharp peak at 3.38 ppm was assigned to the three protons in the methoxyl group of the PEG chain end, and the peak at 3.45 ppm was assigned to the two protons in the carbon next to the hydroxyl group ($-\boldsymbol{CH_2}-$OH) of aminopentanol. Based on their integration area, the addition rate of dodecylamine:PEG:aminopentanol was 1:0.073:0.46 (integration area was 3:0.22:0.92), which was similar to the feeding ratio of these three amines (1:0.074:0.41).

Finally, folate groups were introduced to the amphiphilic poly(β-thiopropionate) by DMAP-catalyzed esterification in anhydrous NMP. After dialysis to remove the unconjugated FAs, the appearance of the peaks in the region 4.3–9.0 ppm confirmed that the folate groups were successfully conjugated onto the amphiphilic polymers, as shown in Figure S1D. After conjugation with FA, the grafting ratio of FA could be calculated from the comparison of the peak at 8.66 ppm, attributed to the only proton on the hetero ring of folate, with the peak at 0.86 ppm from the methyl groups of dodecylamine. The calculated ratio of dodecylamine and folate was 1:0.5 (integration intensity is 3:0.5); therefore, the ratio of folate and aminopentanol was 1.09:1, which suggested that most hydroxyl groups on the copolymers were conjugated with folate groups. The hydrophobic alkyl side chains and hydrophilic PEG side chains helped the amphiphilic copolymers form stabilized micelles for drug loading in aqueous solution. In the low-pH environment of tumor sites, poly(β-thiopropionate) amphiphilic copolymers could be decomposed into low-MW segments through

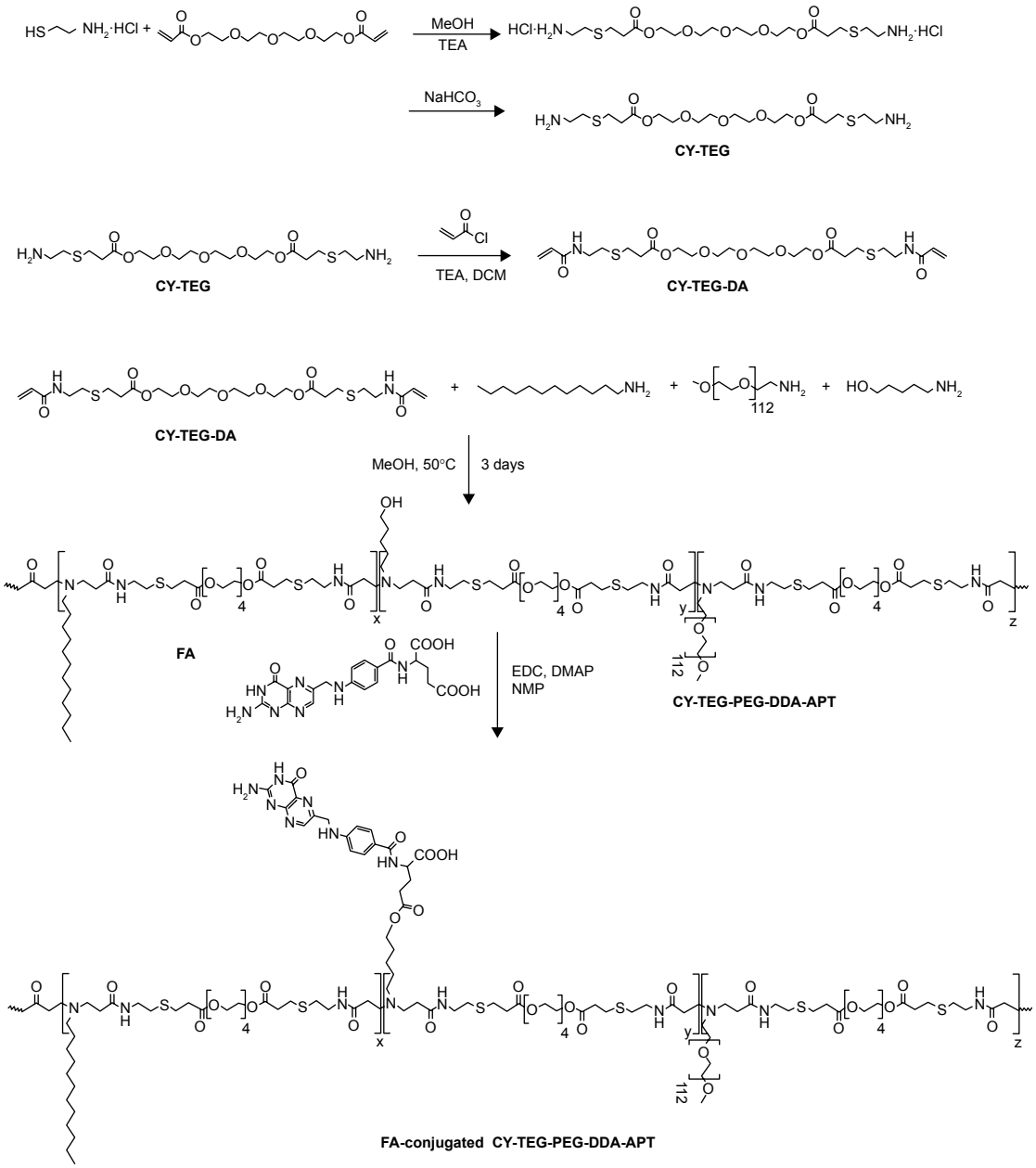

Figure 1 Synthetic route of folate-conjugated amphiphilic poly(β-thiopropionate).
Abbreviations: FA, folic acid; TEA, trimethylamine; DCM, dichloromethane; NMP, N-methyl-2-pyrrolidone; EDC, 1-ethyl-3-(3-dimethylaminopropyl) carbodiimide; DMAP, 4-dimethylaminopyridine; PEG, polyethylene glycol; MeOH, methanol; CY, cysteamine; TEG, tetra (ethylene glycol); CY-TEG, cysteamine capped tetra (ethylene glycol); DDA, dodecylamine; APT, 5-aminopentanol; CY-TEG-PEG-DDA-APT, poly (beta-thiopropionate) amphiphilic copolymer.

the cleavage of acid-labile β-thiopropionate backbone linkages to release the drug.[30,31] The protonated tertiary amine groups of the aminoester segments and PEG segments, and other low MW segments, were water soluble and easily metabolized.

TEM observations revealed the morphology of FA-DOX@IONPs, which were shown to be nanoparticles well dispersed without aggregation (Figure 2A). As shown in Figure 2B, DOX released from the FA-DOX@IONPs was measured through dialysis at pH 7.4 and 5.0. Under conditions including a neutral dialysate (pH =7.4), FA-DOX@IONPs displayed a slow and sustained DOX release rate of ~30% within 24 hours, with ~32.5% of DOX released within 48 hours. However, when FA-DOX@IONPs encountered an acidic environment (pH =5.0), the DOX release was more effective than that at pH 7.4, with ~8% release from FA-DOX@IONPs in the first 6 hours, ~51% within 12 hours, and up to ~75% over 48 hours. These results show that FA-DOX@IONPs ensure a smooth and continuous diffusion of DOX in a neutral environment. However, in an acidic

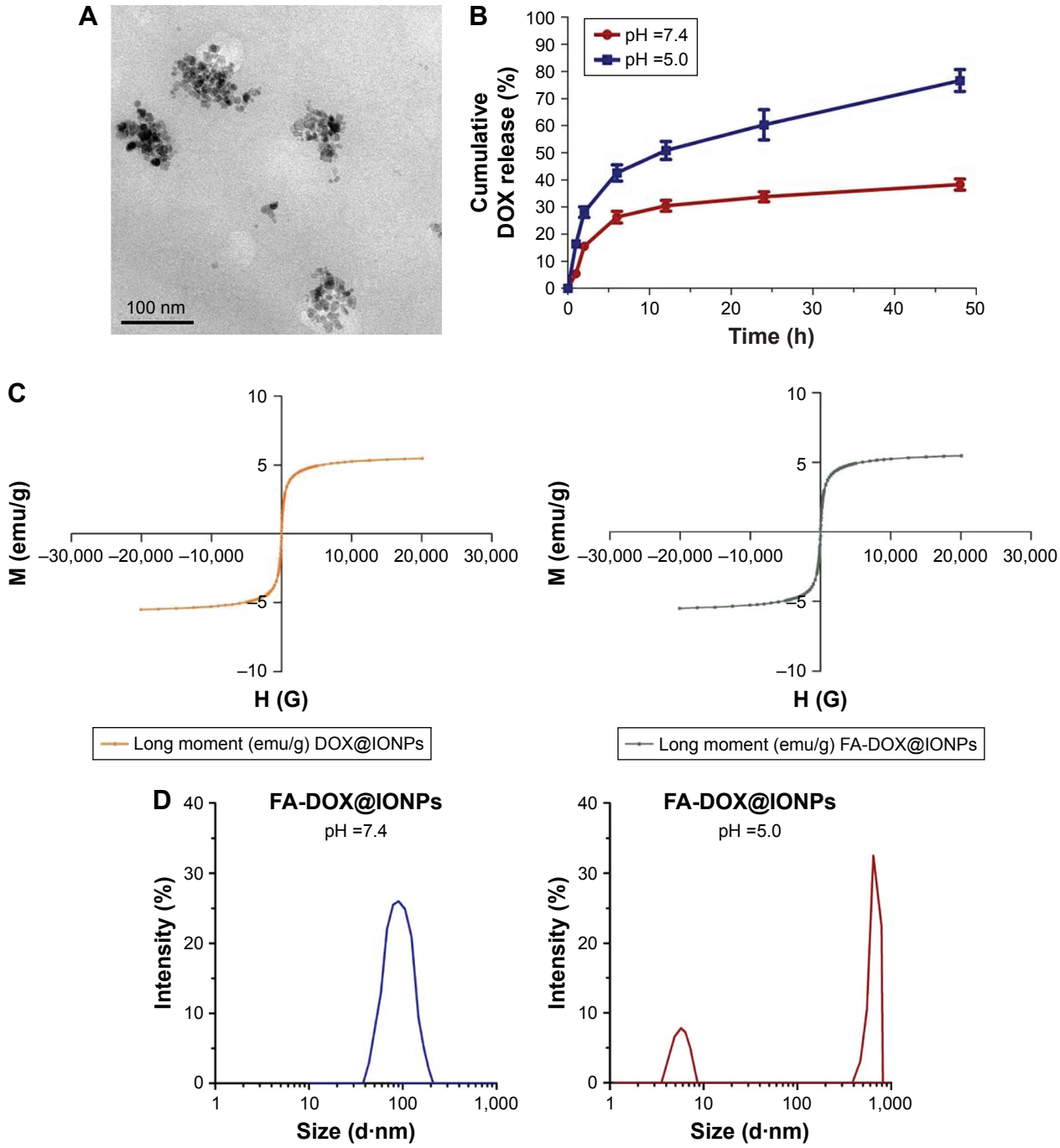

Figure 2 The characterization of synthesized nanoparticles. (**A**) TEM image of nanoparticles; (**B**) pH-dependent DOX release profiles from FA-DOX@IONPs; (**C**) room temperature magnetization curves of synthesized nanoparticles with and without FA coating; and (**D**) the size change of nanoparticles in response to pH decreasing from 7.4 to 5.0 using DLS measurement.

Abbreviations: DOX, doxorubicin; TEM, transmission electron microscopy; FA, folic acid; IONP, iron oxide nanoparticle; DLS, dynamic light scattering.

environment, FA-DOX@IONPs depolymerized faster and released DOX more rapidly.

The magnetic nature of the nanoparticles was studied through VSM experiments. The magnetization of the nanoparticles is represented as a function of the variation in the magnetic field shown in Figure 2C. The saturation magnetization (σs) of DOX@IONPs and FA-DOX@IONPs was ~5.2 emu/g for both nanoparticles. The M–H curves shown in Figure 2C describe the magnetism of these synthesized magnetic nanoparticles.

As shown in Figure 2D, DLS measurements indicated that the hydrodynamic size of FA-DOX@IONPs was in

the range of 40−200 nm (~100 nm) in neutral conditions (pH =7.4). The size changes of the nanoparticles in response to an acidic environment (pH =5.0) were also observed by DLS. After the adjustment of the pH value of the solution to 5.0, the dissolution of the nanoparticles was observed corresponding to the peak up to 600 nm in diameter and the peak of only ~6 nm in diameter. The size change of the nanoparticles was observed after adjustment of the pH value and reflected the aggregation and dissolution of the nanoparticles. Given that such hydrodynamic size changes occurred in response to the pH value, FA-DOX@IONPs were confirmed to be suitable for DOX delivery to the intrinsic acidic environment of tumors.

FR expression of breast cancer cells

The targeting of FR is a valid approach to increase the transport of drug-loaded nanoparticles to cancerous cells, such as breast cancer cells (highly FR overexpressing).[32] We first investigated the FR protein expression in the human breast carcinoma cell lines (BT549, MCF-7, and MDA-MB-231) by Western blot assay. FR protein expression was detected in all three cell lines (Figure S2). The MCF-7 human breast cancer cell line, which had the strongest intensity of FR protein expression (Figure S2), was selected as the candidate for our subsequent studies.

FA-DOX@IONP-mediated breast cancer cells apoptosis

The anti-carcinoma effect arises from drug-induced cancer cell apoptosis.[33] The antineoplastic medicine DOX can distort a group of normal chromosomes into aberrant chromatin clumps, thereby causing inhibition of DNA and RNA synthesis when DOX enters a tumor cell nucleus.[34] The above process is known as apoptosis, and chromatin clumps are used commonly as a marker of drug-induced tumor cell apoptosis.[35] Hence, the DOX-carrying nanoclusters were observed by TEM to determine their apoptotic effects on MCF-7 breast cancer cells (Figure 3). The distorted chromatin clumps (white arrow in Figure 3A and B) and the produced lipid droplets (black arrow in Figure 3A and B) both confirmed the occurrence of FA-DOX@IONP-mediated apoptosis. As shown in Figure 3C and D, the FA-DOX@

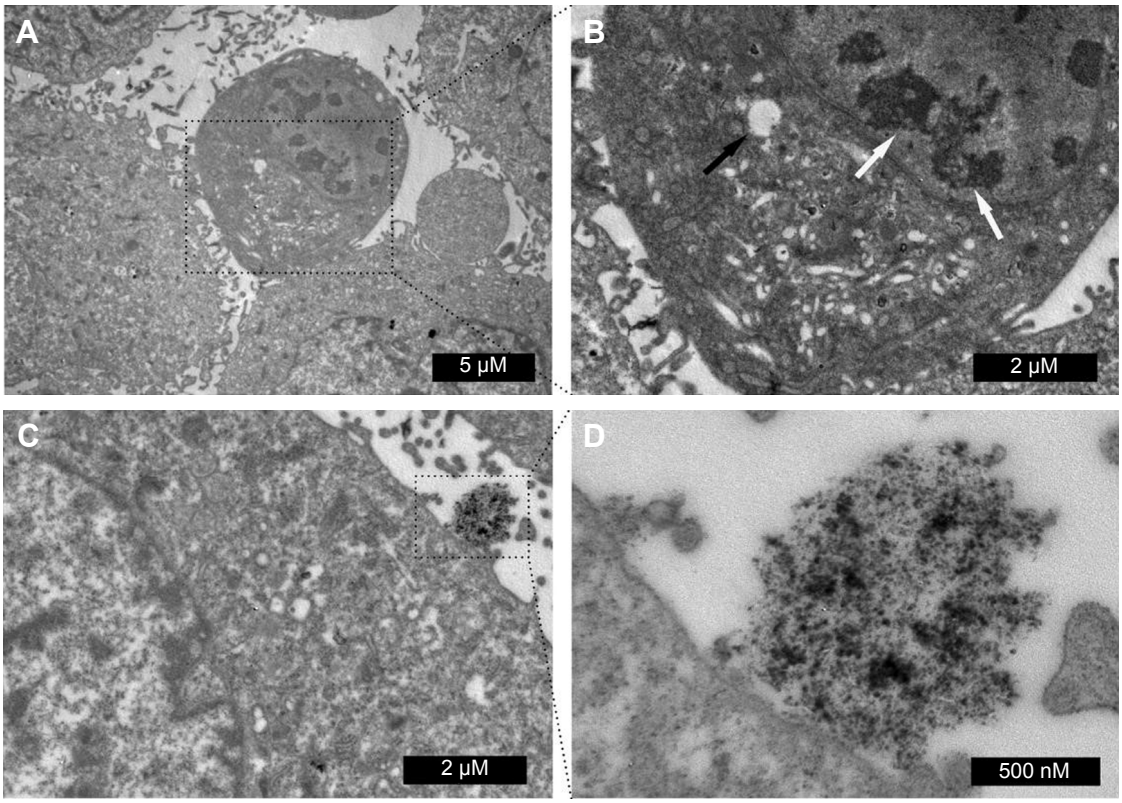

Figure 3 TEM investigation of FA-DOX@IONP-mediated cell apoptosis. (**A**, **B**) Intranuclear distorted chromatin clumps are denoted by white arrows and lipid droplet by black arrow. (**C**, **D**) FA-DOX@IONPs and breast cancer cell interaction.
Abbreviations: DOX, doxorubicin; TEM, transmission electron microscopy; FA, folic acid; IONP, iron oxide nanoparticle.

IONPs and breast cancer cells were both found in the intrinsic acidic environment of the tumors.

Cytotoxicity and targeted uptake of DOX, DOX@IONPs, and FA-DOX@IONPs in vitro

In order to verify the targeting efficacy of nanoparticles, the CCK8 assay was conducted to estimate the viability of MCF-7 cells in FA-free media: DOX, DOX@IONPs, and FA-DOX@IONPs were used, with DOX concentrations of 1, 2.5, 5, 10, and 15 μg/mL, in FA-free media (pH 7.4) for 24 hours. As the DOX concentration increased, a gradually decreasing trend in the cell viability with all treatments was observed. We found that the cell viability of DOX@IONP-treated cells was higher than that of only DOX-treated cells, but the difference was not statistically significant; this may be explained by the action of a small-molecule drug, such as DOX, which can easily diffuse into MCF-7 cells to exert an inhibitory effect on the cells, whereas the macromolecular nanoparticles, such as DOX@IONPs, must be translocated across the plasma membrane by endocytosis. However, the viability of the FA-DOX@IONP-treated cells was lower than that of the other two groups ($p<0.05$). This may result from the FRs expressed on MCF-7 cells, as shown in Figure S2. The active targeting of FA-conjugated nanoparticles led to more successful transport through the cellular membrane. The half inhibitory concentration of DOX, DOX@IONPs, and FA-DOX@IONPs at 24 hours was ~6.0, ~10.0, and ~2.8 μg/mL, respectively.

Further fluorescent images provided evidence that FA conjugation improved the efficacy of intracellular delivery. MCF-7 cells were exposed to DOX, DOX@IONPs, and FA-DOX@IONPs at an equivalent DOX concentration (7.5 μg/mL) for 2, 12, and 24 hours at pH 7.4 (Figure 4). DOX, a red fluorescent chemotherapeutic drug, mainly enters the cell nucleus to inhibit nuclear DNA replication.[36] As time progressed, the red fluorescent intensity strengthened in all treatments and a decrease in MCF-7 cells was observed, as shown in Figure 4A. The red fluorescence intensities of pure DOX and DOX@IONPs were clearly weaker than that observed in FA-DOX@IONP-treated cells, which may be attributable to the effective FR targeting of the nanoparticles. This was similar to the results of the CCK8 assay (Figure 5). Additionally, gastric cancer cell nuclei were stained with DAPI (Figure 4B, blue, left panel), and the membranes and cytoplasm were stained with DIO (Figure 4B, green, right panel).

Antitumor effects on breast cancer xenograft model in vivo

It has been proven that the human breast cancer cell line MCF-7 expresses the FR protein; therefore, the antitumor effects of FA-DOX@IONPs combined with MRI and the external magnetic force in vivo were examined in female nude mice xenografted with MCF-7 tumors. The tumor growth curves (Figure 6A) showed that the drug-treated groups, including DOX (group 2), DOX@IONPs (group 3), FA-DOX@IONPs (group 4), DOX@IONPs plus magnetic treatment (group 5), and FA-DOX@IONPs plus magnetic treatment (group 6), were used to study tumor growth suppression through comparison with the PBS-treated control group (group 1). The xenografted tumors of mice in group 2 grew more slowly than those of group 1, which proved that DOX was an effective inhibitor of tumor growth. Unfortunately, there were no statistical differences between groups 2 and 3 with regard to tumor growth, which suggested that DOX@IONPs offer few advantages over pure DOX in vivo, although DOX@IONPs appeared to exert more powerful antitumor effects than DOX owing to the intrinsic acidic tumor environment. However, when nanoparticles were entrapped with FA and/or enhanced by magnetism, significant inhibition of breast tumor growth was observed in groups 4, 5, and 6 compared with group 2 after 24 days of treatment ($p<0.05$), which suggested greater antitumor effectiveness of DOX-loaded nanoparticles enhanced by FA targeting and/or magnetism than pure DOX. Interestingly, similar antitumor efficacy was found in groups 4 and 5 when mice were treated with FA-DOX@IONPs and DOX@IONPs plus magnetism, respectively, which indicated that magnetic induction and FA targeting may share a similar antitumor ability in vivo. Moreover, FA-DOX@IONPs plus magnetic treatment (group 6) caused a marked delay in tumor growth compared to that in other groups ($p<0.05$), which may be explained by the entrapped FA in the nanoparticles, the application of the external magnetic force, and the intrinsic acidic tumor environment. FA-DOX@IONPs plus magnetic treatment (group 6) markedly suppressed tumor growth from day 6 to the endpoint in contrast to the DOX solution (group 2) ($p<0.05$), which suggested that FA-DOX@IONPs plus magnetic treatment could quickly and durably suppress breast tumor growth.

After 24 days of treatment, the average size of the tumor mass in group 1 increased by 2,048.08%±59.99% and by 1,421.26%±94.48% in group 2, as shown in Figure 6C. Compared with group 2, the average tumor sizes in groups 3–5 were reduced to 1,225.35%±69.2%, 808.06%±124.29%, and

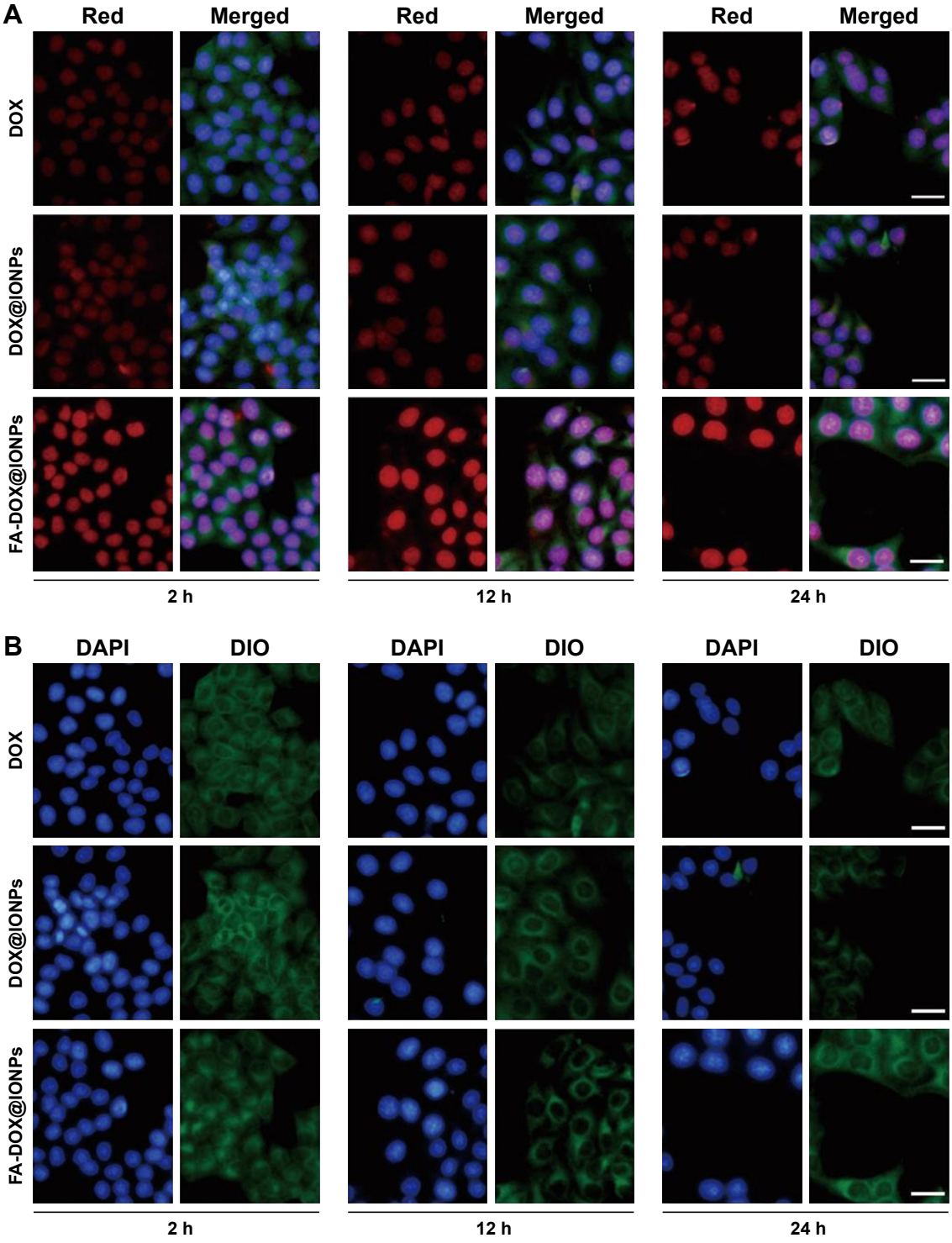

Figure 4 MCF-7 cells incubated with free DOX, DOX@IONPs, and FA-DOX@IONPs (at equivalent DOX concentration of 7.5 μg/mL). (**A**) DOX fluorescence is red (in the left panel), cell nuclei were stained with blue using DAPI, and the membranes and cytoplasm were stained with green using DIO. Merged images are shown in the right panel. (**B**) Fluorescence images with only DAPI and DIO staining. Scale bars =20 μm.
Abbreviations: DOX, doxorubicin; FA, folic acid; IONP, iron oxide nanoparticle; DIO, 3,3′-dioctadecyloxacarbocyanine perchlorate; DAPI, 4′,6-diamidino-2-phenylindole.

838.99%±88.29%, respectively. The average size of the transplanted tumors significantly decreased to 219.32%±58.21% when the mice were subjected to FA-DOX@IONPs plus magnetic treatment in group 6, compared to that of group 2 ($p<0.05$). We also studied the influence of the nanoparticles on mice weight and found no apparent decreases in body weight in all groups, as shown in Figure 6B. In addition, the body weight of mice showed a slowly increasing trend in all

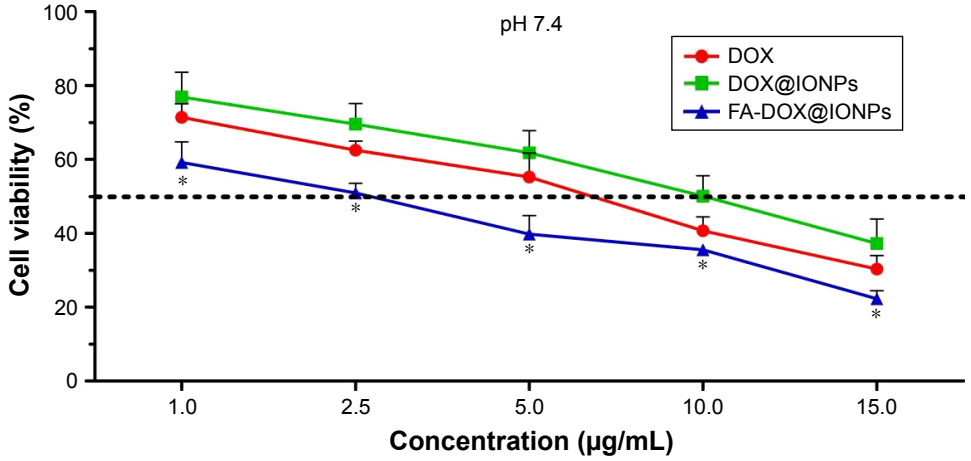

Figure 5 Viability of MCF-7 cells subjected to DOX, DOX@IONPs, and FA-DOX@IONPs, respectively, at DOX concentrations (1, 2.5, 5, 10, and 15 μg/mL) for 24 hours measured by CCK8 assay. *$p<0.05$ is considered to be a statistically significant difference (n=3).
Abbreviations: DOX, doxorubicin; FA, folic acid; IONP, iron oxide nanoparticle; CCK8, cell counting kit-8.

groups (without statistical significance), perhaps because of the high tumor burden. Moreover, no obvious pathological changes were detected in the hearts, livers, and kidneys in all groups by H&E staining (Figure 7); these results may be explained by the short course of DOX treatment in the xenograft model in vivo and/or the poor sensitivity of H&E staining. FA-DOX@IONPs or DOX@IONPs did not increase the side effects of DOX. Additionally, no obvious iron depositions were observed in the tumors or the hearts, livers, and kidneys after 24 days of FA-DOX@IONPs

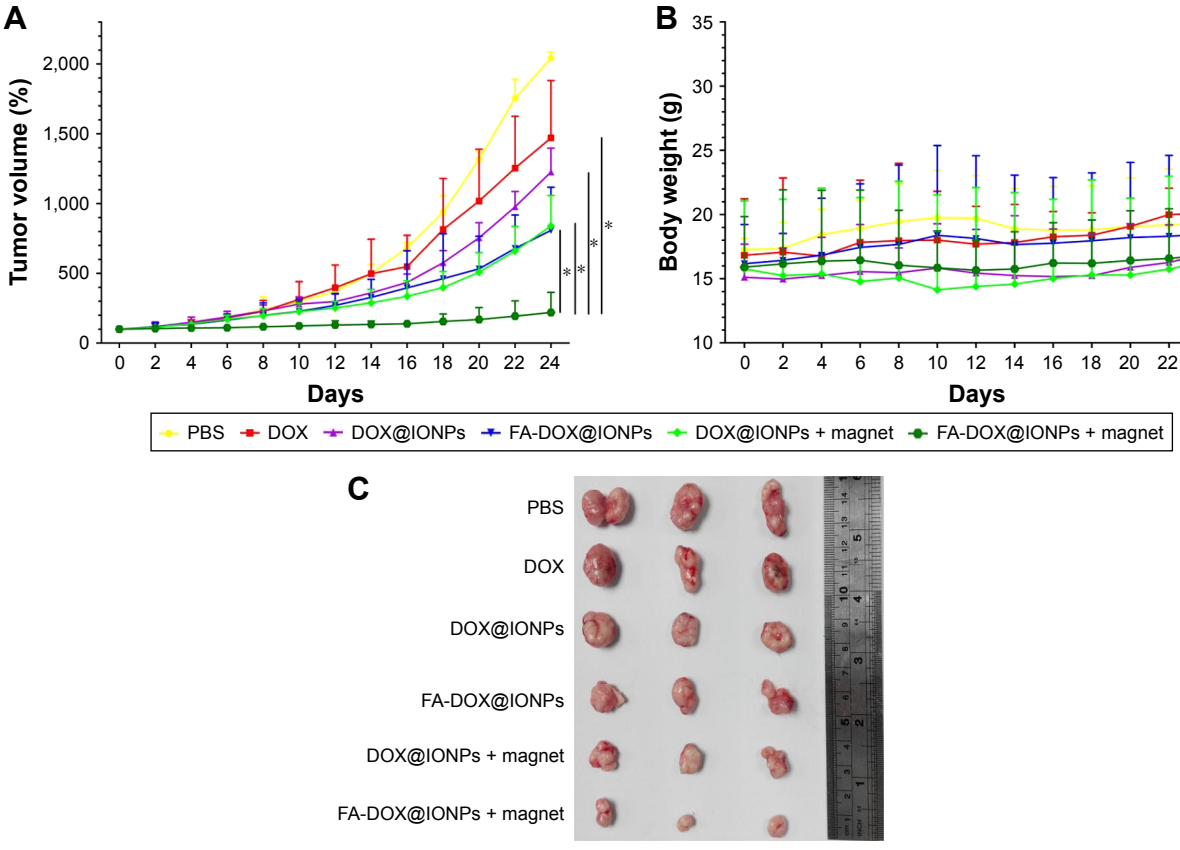

Figure 6 Antitumor efficacy of targeting-active and external magnetic nanoparticles in vivo. (**A**) Tumor growth curve of PBS, DOX, DOX@IONPs, FA-DOX@IONPs, DOX@IONPs plus magnetic treatment, and FA-DOX@IONPs plus magnetic treatment. *$p<0.05$ is considered to be a statistically significant difference (n=3). (**B**) The body weight changes with the treatments for 24 days. (**C**) Tumor size on the 24th day after treatment of PBS, DOX, DOX@IONPs, FA-DOX@IONPs, and DOX@IONPs plus magnetic treatment.
Abbreviations: DOX, doxorubicin; FA, folic acid; IONP, iron oxide nanoparticle.

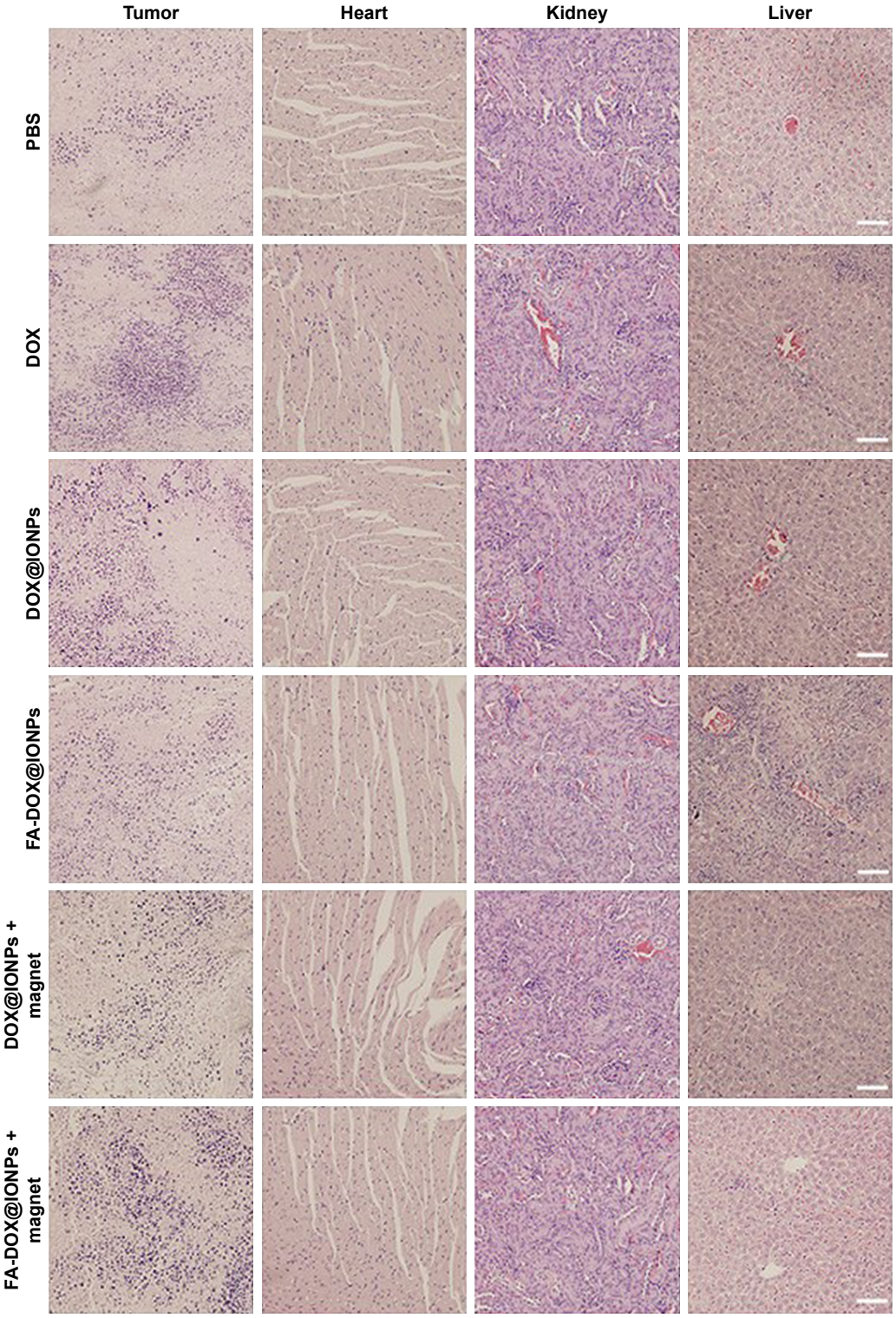

Figure 7 H&E staining micrographs (×200) of tumor sections, heart, kidney, and liver from PBS, free DOX, DOX@IONPs, FA-DOX@IONPs, DOX@IONPs plus magnetic treatment, and FA-DOX@IONPs plus magnetic treatment groups on day 24. Scale bars =50 μm.
Abbreviations: DOX, doxorubicin; FA, folic acid; IONP, iron oxide nanoparticle.

or DOX@IONPs treatments by Prussian blue staining (Figure 8), which suggested that the nanoparticles were effectively biodegraded. It is known that the liver could phagocytize FA-DOX@IONPs, and plays a main role in the metabolism of nanomaterials. FA-DOX@IONPs were shown to be phagocytosed by the liver within the first 36 hours in the MRI, and appeared as round dark areas (Figure 9), but the Prussian blue staining disappeared by day 24 because of

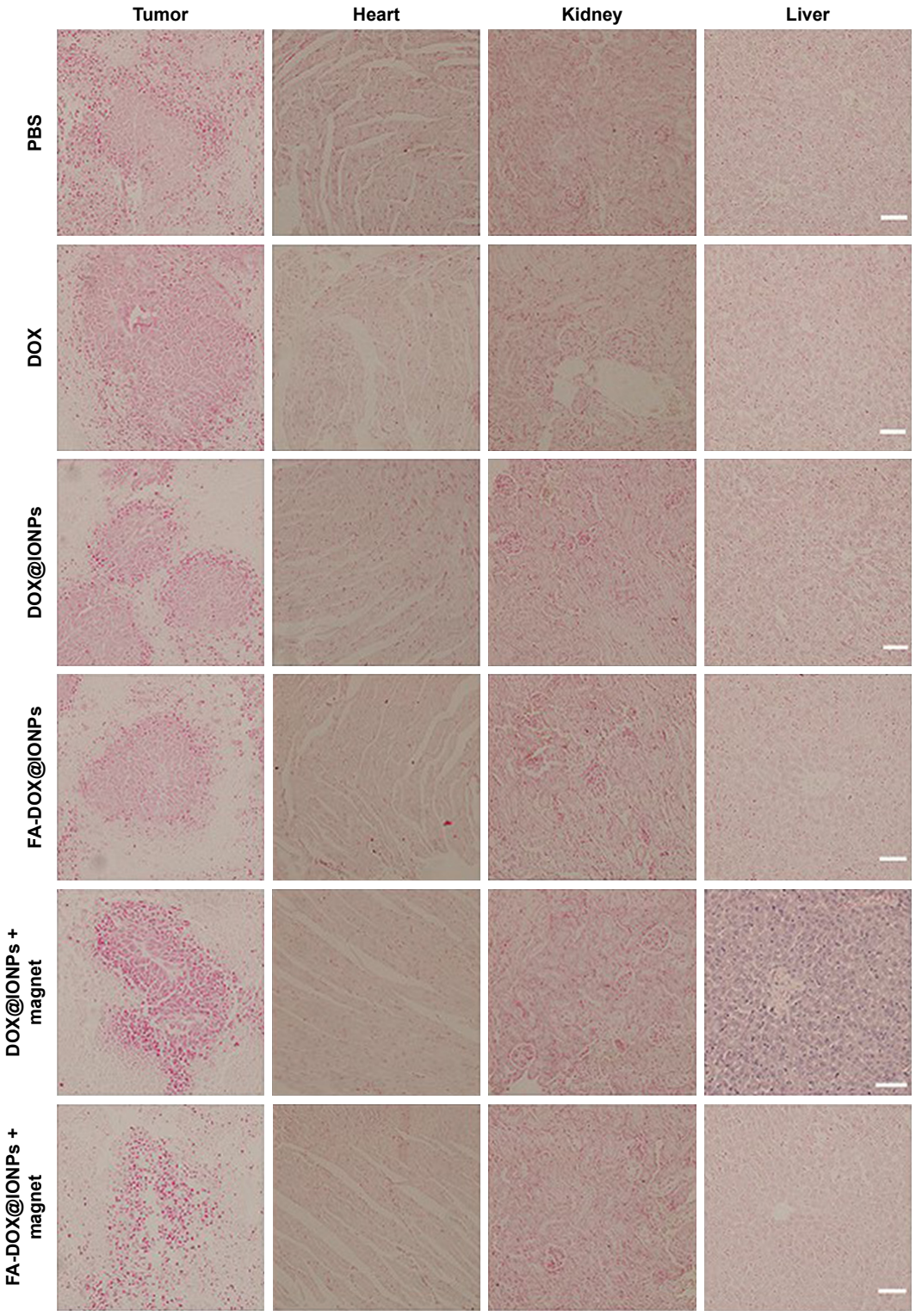

Figure 8 Prussian blue micrographs (×200) of tumor sections, heart, kidney, and liver from PBS, free DOX, DOX@IONPs, FA-DOX@IONPs, DOX@IONPs plus magnetic treatment, and FA-DOX@IONPs plus magnetic treatment groups on day 24. Scale bars =50 μm.
Abbreviations: DOX, doxorubicin; FA, folic acid; IONP, iron oxide nanoparticle.

biodegradation. Iron deposition also disappeared in the hearts and kidneys on day 24, as observed by Prussian blue staining. These results confirmed that DOX@IONPs and FA-DOX@IONPs exerted no apparent disadvantages on the organs of healthy mice after 24 days of treatment. Collectively, both FA-DOX@IONPs and DOX@IONPs were shown to have low toxicity and to be highly biodegradable, which indicated their safety for clinical practice.

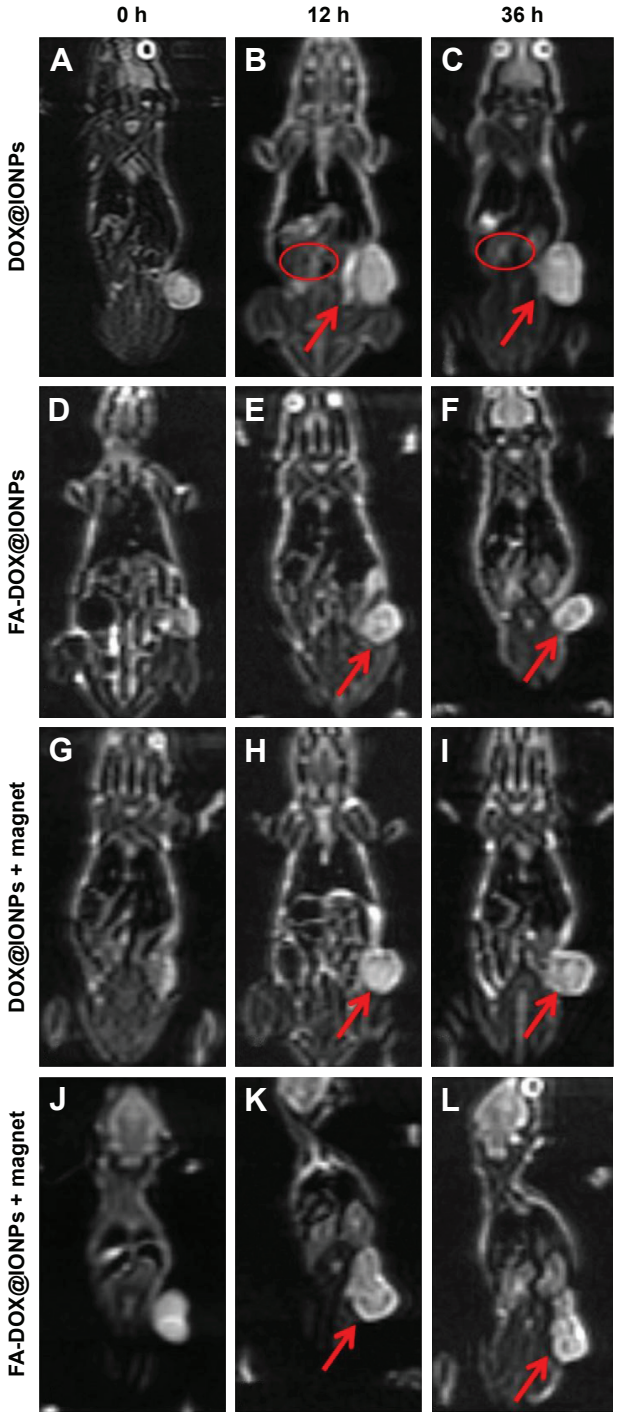

Figure 9 Coronal T2 weighted images of mice after injection at 0, 12, and 36 hours. Coronal T2 weighted images of mice after injection of (**A–C**) DOX@IONPs; (**D–F**) FA-DOX@IONPs; (**G–I**) DOX@IONPs plus magnetic field (magnet); and (**J–L**) FA-DOX@IONPs plus magnetic field. The red arrows denote the tumor site and red circles denote the liver of the mouse.
Abbreviations: DOX, doxorubicin; FA, folic acid; IONP, iron oxide nanoparticle.

MRI of DOX@IONPs and FA-DOX@IONPs in vivo

MRI can visualize iron oxide, a contrast agent that possesses high sensitivity to the spin-echo T2-weighted image. Both FA-DOX@IONPs and DOX@IONPs contained iron oxide, and thus could be captured by the low signal of a T2-weighted image. The T2-weighted coronal and axial MRI images of the mice before and after the nanoparticle injection at 12 and 36 hours are presented in Figure 9. When compared with the mice before nanoparticle injection, all treatments revealed varying degrees of rounded dark areas in the tumor (red arrows), denoting the aggregation of magnetic IONPs at the tumor sites at 12 and 36 hours after treatment. In addition, in contrast with images captured after 12 hours, darker, round areas on the tumor sites were obtained by MRI at 36 hours after administration in each treatment group. Moreover, the FA-DOX@IONPs plus magnetic treatment (Figure 9J–L) group displayed the strongest and largest presence at the tumor site at both time points in contrast with the other treatment groups, DOX@IONPs (Figure 9A–C), FA-DOX@IONPs (Figure 9D–F), and DOX@IONPs plus magnetic treatment (Figure 9G–I). The results showed that FA-DOX@IONPs with FA targeting and pH-sensibility could be directed to the tumor area more efficiently than DOX@IONPs under an externally applied magnetic field. As shown in Figure 9B, some dark areas (red circles) appeared on the liver, where these nanoparticles were taken up after the injection of DOX@IONPs at 12 hours. However, the darkness decreased slightly in the liver after 36 hours (Figure 9C) owing to the gradual decomposition of the nanoparticles, as previously mentioned. A homologous phenomenon occurred in mice tumor sites, in which a slight recession of the dark fields emerged in the T2-weighted images, which was also attributed to the degradation of the FA-DOX@IONPs and DOX@IONPs. In addition to the antitumor effects in vitro and in vivo, these results indicated that FA-DOX@IONPs not only inhibited breast cancer cells proliferation through apoptosis, but could also be monitored by MRI imaging, which is convenient for the clinical treatment of breast cancer.

Inhibition of tumor microvascular generation

Neovascularization is the fundamental process of tumor growth and expansion that provides plentiful nutrients, oxygen, and favorable environmental stimuli.[37] CD31 expression is related to tumor neovascularization and is often used as a tumor endothelial marker. Thus, tumor angiogenesis of treated mice was determined by CD31 immunohistochemistry, which was then used for the estimation of AMVD. The micrographs of CD31 immunohistochemical staining of breast cancer cells in mice subjected to PBS (Figure 10A), DOX (Figure 10B), DOX@IONPs (Figure 10C), FA-DOX@IONPs (Figure 10D), DOX@IONPs plus magnetic treatment (Figure 10E), and FA-DOX@IONPs plus magnetic treatment

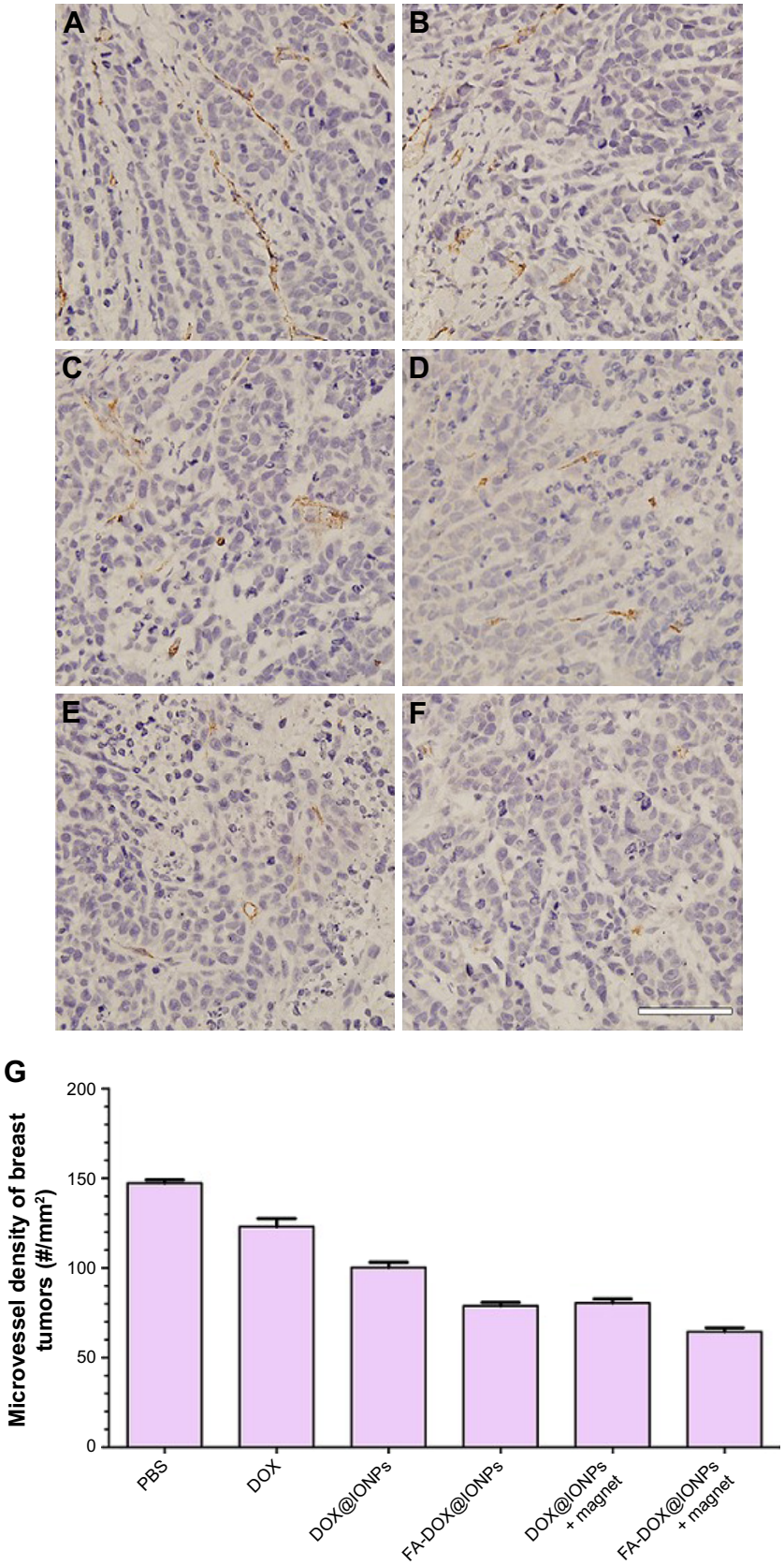

Figure 10 Representative micrographs of CD31 immunohistochemistry of breast cancer cells in mice treated with (**A**) PBS, (**B**) free DOX, (**C**) DOX@IONPs, (**D**) FA-DOX@IONPs, (**E**) DOX@IONPs plus magnetic treatment, and (**F**) FA-DOX@IONPs plus magnetic treatment. (**G**) Microvascular vessels staining and AMVD (the number of microvessels per mm^2) of mice breast cancer tumors. Scale bar =100 μm.

Abbreviations: DOX, doxorubicin; FA, folic acid; IONP, iron oxide nanoparticle; AMVD, average microvessel density.

(Figure 10F) are shown in Figure 10. The AMVD in these six groups was 147.20±4.14, 122.40±4.93, 100.20±6.72, 78.80±4.32, 80.40±5.32, and 64.40±4.83 /mm^2, respectively, as shown in Figure 10G. Although the DOX-treated tissues showed significant inhibition compared with PBS-treated tissues, CD31 expression clearly indicated that nanoparticle-treated tumors had even fewer intratumoral microvessels than in the DOX group ($p<0.05$). The FA conjugation and external magnetic guidance appeared to have fairly similar antiangiogenic effects, with their contribution through the combination of magnetic force and active targeting in FA-DOX@IONPs demonstrating the most efficient inhibition of microvessels, which corresponded well with the antitumor effects observed in vitro and in vivo.

Conclusion

In this study, we successfully synthesized polyfunctional magnetized FA-DOX@IONPs with FR-targeting specificity and pH sensitivity. Our current study indicated the clear advantages of FA-DOX@IONPs in comparison with free DOX or DOX@IONPs for the treatment of breast carcinoma without discernible side effects. Furthermore, the established and relevant MRI technology could be readily used to orientate FA-DOX@IONPs for preferable diagnosis and treatment of breast cancer. In conclusion, FA-DOX@IONPs equipped with dual targeting methods and pH-sensitive capacity are a promising theranostic candidate for breast cancer, although more research may be required to completely elucidate their clinical applications.

Acknowledgments

Our study was supported by the National Natural Science Foundation of China (81472314), NSERCNSERC Discovery Grant, NSERC Discovery Accelerator Supplements, Manitoba RPP, and the Natural Science Foundation of Guangdong Province (2014A030313272). We thank Dr Wang for the MRI measurements, which were performed at The Imaging Center, 999 Brain Hospital, Guangzhou, China.

Disclosure

The authors report no conflicts of interest in this work.

References

1. Rugo HS. Hormone therapy in premenopausal women with early-stage breast cancer. *N Engl J Med*. 2014;371:175–176.
2. Ahmed M, Purushotham AD, Douek M. Novel techniques for sentinel lymph node biopsy in breast cancer: a systematic review. *Lancet Oncol*. 2014;15:e351–e362.
3. DeSantis C, Ma J, Bryan L, Jemal A. Breast cancer statistics, 2013. *CA Cancer J Clin*. 2014;64:52–62.
4. Peto R, Davies C, Godwin J, et al. Comparisons between different polychemotherapy regimens for early breast cancer: meta-analyses of long-term outcome among 100,000 women in 123 randomised trials. *Lancet*. 2012;379:432–444.
5. Arola OJ, Saraste A, Pulkki K, Kallajoki M, Parvinen M, Voipio-Pulkki LM. Acute doxorubicin cardiotoxicity involves cardiomyocyte apoptosis. *Cancer Res*. 2000;60:1789–1792.
6. Keefe DL. Anthracycline-induced cardiomyopathy. *Semin Oncol*. 2001;28:2–7.
7. Swain SM, Whaley FS, Ewer MS. Congestive heart failure in patients treated with doxorubicin: a retrospective analysis of three trials. *Cancer*. 2003;97:2869–2879.
8. Singal PK, Iliskovic N. Doxorubicin-induced cardiomyopathy. *N Engl J Med*. 1998;339:900–905.
9. Ng R, Green MD. Managing cardiotoxicity in anthracycline-treated breast cancers. *Expert Opin Drug Saf*. 2007;6:315–321.
10. Von Hoff DD, Layard MW, Basa P, et al. Risk factors for doxorubicin-induced congestive heart failure. *Ann Intern Med*. 1979;91:710–717.
11. Alexander J, Dainiak N, Berger HJ, et al. Serial assessment of doxorubicin cardiotoxicity with quantitative radionuclide angiocardiography. *N Engl J Med*. 1979;300:278–283.
12. Zeglinski M, Ludke A, Jassal DS, Singal PK. Trastuzumab-induced cardiac dysfunction: a 'dual-hit'. *Exp Clin Cardiol*. 2011;16:70–74.
13. Peer D, Karp JM, Hong S, Farokhzad OC, Margalit R, Langer R. Nanocarriers as an emerging platform for cancer therapy. *Nat Nanotechnol*. 2007;2:751–760.
14. Davis ME, Chen ZG, Shin DM. Nanoparticle therapeutics: an emerging treatment modality for cancer. *Nat Rev Drug Discov*. 2008;7:771–782.
15. Singh R, Lillard JW Jr. Nanoparticle-based targeted drug delivery. *Exp Mol Pathol*. 2009;86:215–223.
16. Park TG. Perfusion culture of hepatocytes within galactose-derivatized biodegradable poly(lactide-co-glycolide) scaffolds prepared by gas foaming of effervescent salts. *J Biomed Mater Res*. 2002;59:127–135.
17. Chen J, Qiu X, Ouyang J, Kong J, Zhong W, Xing MM. pH and reduction dual-sensitive copolymeric micelles for intracellular doxorubicin delivery. *Biomacromolecules*. 2011;12:3601–3611.
18. Corot C, Robert P, Idee JM, Port M. Recent advances in iron oxide nanocrystal technology for medical imaging. *Adv Drug Deliv Rev*. 2006;58:1471–1504.
19. Gupta AK, Gupta M. Synthesis and surface engineering of iron oxide nanoparticles for biomedical applications. *Biomaterials*. 2005;26:3995–4021.
20. Babincova M, Altanerova V, Altaner C, Cicmanec P, Babinec P. In vivo heating of magnetic nanoparticles in alternating magnetic field. *Med Phys*. 2004;31:2219–2221.
21. Chen J, Shi M, Liu P, et al. Reducible polyamidoamine-magnetic iron oxide self-assembled nanoparticles for doxorubicin delivery. *Biomaterials*. 2014;35:1240–1248.
22. Murali R, Vidhya P, Thanikaivelan P. Thermoresponsive magnetic nanoparticle-aminated guar gum hydrogel system for sustained release of doxorubicin hydrochloride. *Carbohydr Polym*. 2014;110:440–445.
23. Kaminskas LM, McLeod VM, Porter CJ, Boyd BJ. Association of chemotherapeutic drugs with dendrimer nanocarriers: an assessment of the merits of covalent conjugation compared to noncovalent encapsulation. *Mol Pharm*. 2012;9:355–373.
24. Quintana A, Raczka E, Piehler L, et al. Design and function of a dendrimer-based therapeutic nanodevice targeted to tumor cells through the folate receptor. *Pharm Res*. 2002;19(9):1310–1316.
25. Myc A, Douce TB, Ahuja N, et al. Preclinical antitumor efficacy evaluation of dendrimer-based methotrexate conjugates. *Anticancer Drugs*. 2008;19:143–149.
26. Singh P, Gupta U, Asthana A, Jain NK. Folate and folate-PEG-PAMAM dendrimers: synthesis, characterization, and targeted anticancer drug delivery potential in tumor bearing mice. *Bioconjug Chem*. 2008;19:2239–2252.

27. Chen J, Chen H, Li P, et al. Simultaneous regeneration of articular cartilage and subchondral bone in vivo using MSCs induced by a spatially controlled gene delivery system in bilayered integrated scaffolds. *Biomaterials*. 2011;32:4793–4805.
28. Oishi M, Nagasaki Y, Itaka K, Nishiyama N, Kataoka K. Lactosylated poly(ethylene glycol)-siRNA conjugate through acid-labile beta-thiopropionate linkage to construct pH-sensitive polyion complex micelles achieving enhanced gene silencing in hepatoma cells. *J Am Chem Soc*. 2005;127:1624–1625.
29. Nicolaides NC, O'Shannessy DJ, Albone E, Grasso L. Co-development of diagnostic vectors to support targeted therapies and theranostics: essential tools in personalized cancer therapy. *Front Oncol*. 2014;4:141.
30. Oishi M, Sasaki S, Nagasaki Y, Kataoka K. pH-responsive oligodeoxynucleotide (ODN)-poly(ethylene glycol) conjugate through acid-labile beta-thiopropionate linkage: preparation and polyion complex micelle formation. *Biomacromolecules*. 2003;4:1426–1432.
31. Zou J, Zhang FW, Zhang SY, et al. Poly(ethylene oxide)-block-polyphosphoester-graft-paclitaxel conjugates with acid-labile linkages as a pH-sensitive and functional nanoscopic platform for paclitaxel delivery. *Adv Healthc Mater*. 2014;3:444–448.
32. Tavassolian F, Kamalinia G, Rouhani H, et al. Targeted poly (L-gamma-glutamyl glutamine) nanoparticles of docetaxel against folate over-expressed breast cancer cells. *Int J Pharm*. 2014;467:123–138.
33. Ueno M, Kakinuma Y, Yuhki K, et al. Doxorubicin induces apoptosis by activation of caspase-3 in cultured cardiomyocytes in vitro and rat cardiac ventricles in vivo. *J Pharmacol Sci*. 2006;101:151–158.
34. Szwed M, Laroche-Clary A, Robert J, Jozwiak Z. Induction of apoptosis by doxorubicin-transferrin conjugate compared to free doxorubicin in the human leukemia cell lines. *Chem Biol Interact*. 2014;220:140–148.
35. Wang D, Xu Z, Yu H, et al. Treatment of metastatic breast cancer by combination of chemotherapy and photothermal ablation using doxorubicin-loaded DNA wrapped gold nanorods. *Biomaterials*. 2014;35:8374–8384.
36. Cutts SM, Nudelman A, Rephaeli A, Phillips DR. The power and potential of doxorubicin-DNA adducts. *IUBMB Life*. 2005;57:73–81.
37. Folkman J. Angiogenesis and breast cancer. *J Clin Oncol*. 1994;12:441–443.

Supplementary materials

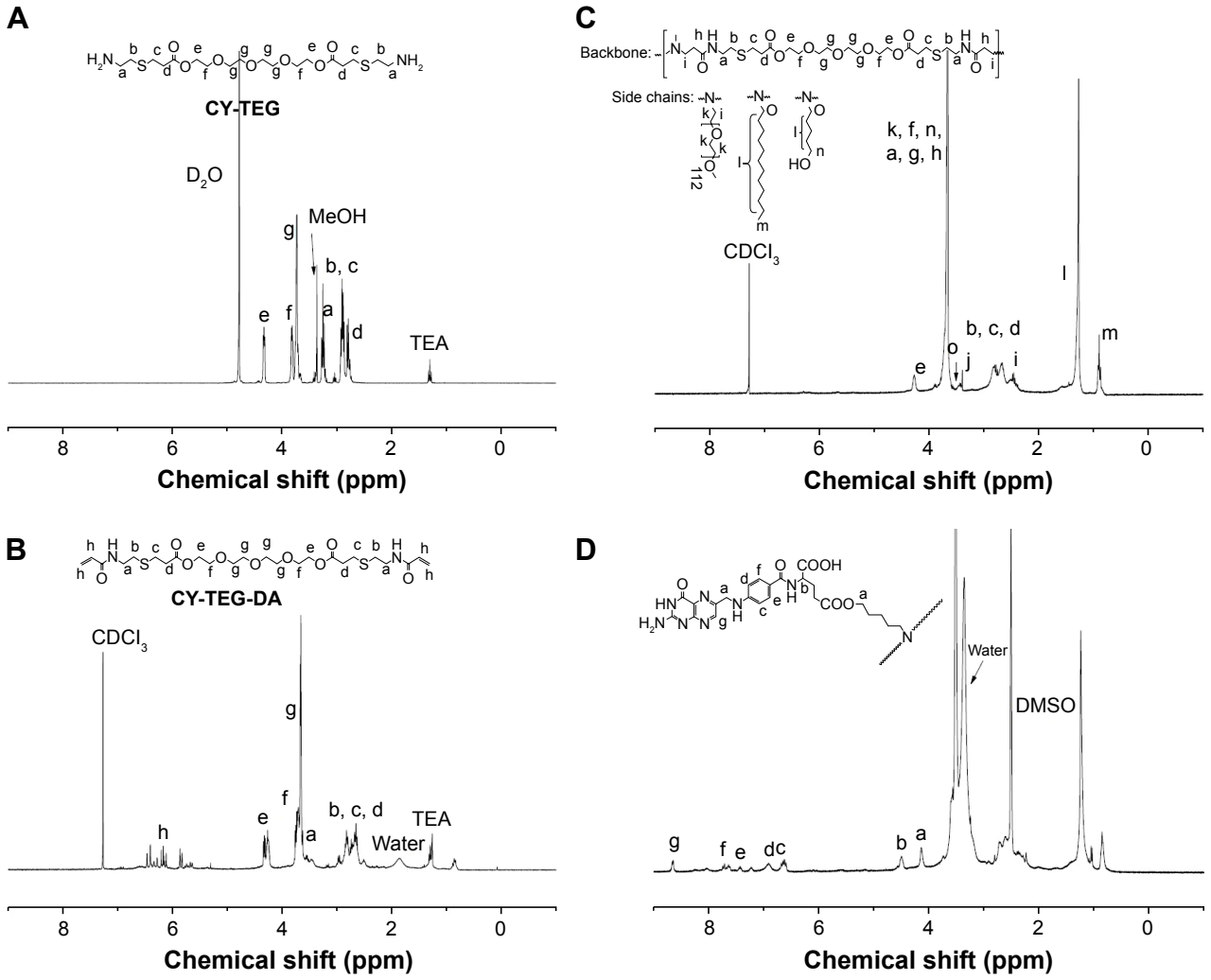

Figure S1 ^{1}H NMR spectrum analysis of (**A**) CY-TEG in D_2O; (**B**) CY-TEG-DA in $CDCl_3$; (**C**) CY-TEG-PEG-DDA-APT (amphiphilic poly (beta-thiopropionate)) in $CDCl_3$; and (**D**) FA conjugated CY-TEG-PEG-DDA-APT (amphiphilic poly (beta-thiopropionate) in DMSO-d_6.

Abbreviations: NMR, nuclear magnetic resonance; TEA, trimethylamine; DMSO, dimethyl sulfoxide; CY-TEG, cysteamine capped tetra (ethylene glycol); DA, diacrylate; PEG, polyethylene glycol; DDA, dodecylamine; APT, 5-aminopentanol; FA, folic acid; MeOH, methanol; CY-TEG-PEG-DDA-APT, poly (beta-thiopropionate) amphiphilic copolymer.

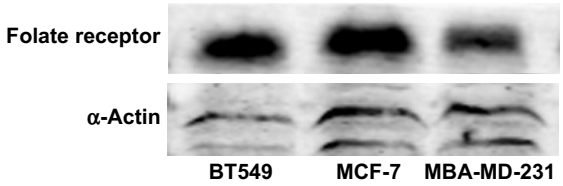

Figure S2 The protein expression of folate receptor in breast cancer cell lines BT549, MCF-7, and MBA-MD-231. α-Actin was used as a loading control.